

Magnetic-field switchable metal-insulator transitions in a quasi-helical conductor

Bernd Braunecker,¹ Anders Ström,² and G. I. Japaridze^{3,4}

¹*Departamento de Física Teórica de la Materia Condensada,*

Facultad de Ciencias, Universidad Autónoma de Madrid, 28049 Madrid, Spain

²*Department of Physics, University of Gothenburg, SE 412 96 Gothenburg, Sweden*

³*Andronikashvili Institute of Physics, Tamarashvili 6, 0177 Tbilisi, Georgia*

⁴*Ilia State University, Cholokashvili Avenue 3-5, 0162 Tbilisi, Georgia*

(Dated: June 15, 2018)

We study Anderson localization in disordered helical conductors that are obtained from one-dimensional conductors with spin-orbit interaction and a magnetic field, or from equivalent systems. We call such conductors “quasi-helical” because the spins of the counterpropagating modes are not perfectly antiparallel and have a small spin-wavefunction overlap that is tunable by the magnetic field. Due to the overlap, disorder backscattering is possible and allows a localization transition. A conductor can pass through two localization transitions with increasing field, one from the conventionally localized system to the quasi-helical conductor (with localization length exceeding the system length), and one at a higher field again to a localized state, due now, however, to backscattering below the magnetic field induced pseudo-gap. We investigate these transitions using a unified two-step renormalization group approach.

I. INTRODUCTION

Over 50 years ago, Anderson showed that a metal-insulator transition can arise due to localization of particles by scattering on a disorder potential.¹ Since then, Anderson localization has evolved into an important topic of condensed matter physics, photonics, and ultra-cold atom gases.² While the basic localization mechanism can be understood on a single-particle basis, a complete investigation needs to include further interactions, especially if they compete against localization. To study such a competition it would be advantageous to control the interactions externally, and to pass through the metal-insulator transition on demand. Here we show that this can indeed be achieved in the presently much investigated one-dimensional (1D) helical conductors through an external magnetic field.

Helical conductors are characterized by spin-filtered transport, in which opposite spins (or Kramers partners) are bound to the right (R) and left (L) moving conduction modes. In conventional 1D conductors, even weak disorder is already sufficient to turn the conductor into an insulator^{3,4} by disorder-induced backscattering between the Fermi points $\pm k_F$. In a helical conductor, however, backscattering is only possible together with a spin-flip, and the conductor is insensitive to normal, spin-preserving disorder scattering.⁵

Helical conductors appear at the edges of topological insulators,⁶ or in quantum wires⁷ or nanotubes⁸ with strong spin-orbit interaction (SOI). They have attracted much attention recently as they allow for spin-filtering,⁷ Cooper pair splitting,⁹ and, if in contact with a superconductor, the realization of Majorana end states.¹⁰ While localization cannot occur in a perfect helical conductor, many of the investigated conductors are imperfect and we call them “quasi-helical”: the spins moving in opposite directions are not perfectly antiparallel. They provide the handle to tune localization externally. Examples are

semiconductor nanowires with strong SOI in the presence of a uniform magnetic field⁷ or, without SOI, of a spiral magnetic field,¹¹ which can also take the form of a spiral Overhauser field due to ordered nuclear spins.¹²

The SOI shifts the spin \uparrow, \downarrow bands by the wave vectors $\pm q_0$ (Fig. 1, dashed lines). A magnetic field B_x perpendicular to the \uparrow, \downarrow axis has now two effects. It lifts the degeneracy at $k = 0$ by opening a pseudo-gap (Fig. 1, solid lines), and it breaks time-reversal symmetry. Tuning the Fermi level to the center of the pseudo-gap by letting $k_F = q_0$ allows conduction only through the modes close to momenta $\pm 2q_0$ with opposite spins. Through B_x , however, these spins are no longer antiparallel, disorder backscattering becomes again possible, and localization can occur.

In this paper we provide a unified approach to such localization, taking into account disorder, magnetic field, spin overlaps, and electron interactions. We formulate a two-step renormalization group (RG) approach within the Luttinger liquid (LL) framework that provides us with a transparent picture of the underlying physics. We consider the zero temperature case, valid if the temperature is smaller than any of the gap sizes.

As a result, we find that varying B_x can cause localization transitions of two kinds. A localized system^{3,4} at $B_x = 0$ can make a transition to a quasi-helical conductor at a critical field B_x^* lying (for the example of InAs nanowires) in the range up to ~ 1 T. This transition is quite abrupt and appears when the B_x generated pseudo-gap overcomes the disorder gap, and the quasi-helical state is lower in energy. The transition is marked by a rapid increase of the localization length ξ_{loc} , and the system is conducting if ξ_{loc} is greater than the system length \mathcal{L} . Through the equal-spin overlap, ξ_{loc} then becomes strongly B_x dependent and decreases with increasing field. At a larger critical field $B_x^{**} > 1$ T, when $\xi_{\text{loc}} < \mathcal{L}$, backscattering between $\pm 2q_0$ causes again localization, resulting in a $4q_0$ modulated density wave co-

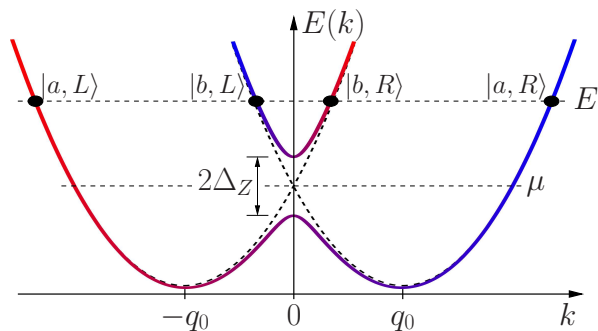


FIG. 1. Electron dispersion for the noninteracting quantum wire with SOI for $B_x = 0$ (dashed lines) and $B_x \neq 0$ (solid lines). The magnetic field opens a pseudo-gap $\Delta_Z = \mu_B g |B_x|/2$ at $k = 0$. We denote the lower (upper) band by a (b). At any energy E the left (L) and right (R) moving states are labeled by $|a/b, L/R\rangle$ as indicated in the figure. The color gradient from red to blue indicates the spin mixing by B_x .

existing with the transverse spin polarization generated by B_x . This coexistence of density wave and uniform polarization distinguishes this phase from conventional localization, and we shall call it “sub-gap localization.” For very strong disorder, the helical phase is suppressed ($B_x^* = B_x^{**}$), and a transition takes place directly between the two localized phases. We show concrete results for InAs nanowires in Sec. VI below. The underlying physics, however, is general and applies to many materials, except for the edge states of topological insulators due to their different band structure. For the latter, quasi-helicity can still be obtained, but has different interesting consequences.¹³

The plan of the remainder of the paper is as follows. In Sec. II we introduce the model of the quasi-helical conductor. The approach for its solution in the presence of disorder is discussed in Sec. III. In Sec. IV we present the necessary background of the bosonization framework, and in Sec. V we discuss the technical details of the two-step RG approach. Section VI contains the discussion of the results for the example of InAs nanowires and the conclusions.

II. MODEL

We consider a generic interacting 1D quantum wire of length \mathcal{L} with SOI and an external magnetic field, described by the Hamiltonian

$$H = \sum_{s,s'} \int dx \psi_s^\dagger(x) \left[\left(\frac{p^2}{2m} - \mu \right) \delta_{s,s'} + \alpha_R \sigma_{s,s'}^z p + \Delta_Z \sigma_{s,s'}^x \right] \psi_{s'}(x) + U_{e-e} + U_{dis}. \quad (1)$$

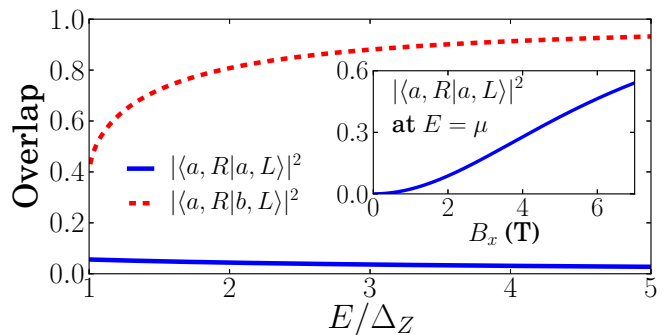


FIG. 2. Overlap integrals $|\langle a, R|a, L\rangle|^2$ and $|\langle a, R|b, L\rangle|^2$ as functions of energy $E > \Delta_Z = \mu_B g |B_x|/2 \approx 0.5$ meV (for InAs with $B_x = 2$ T).¹¹ The states $|a/b, L/R\rangle$ are as indicated in Fig. 1. The inset shows the B_x dependence of $|\langle a, R|a, L\rangle|^2$ at energy $E = \mu$ in the middle of the Δ_Z gap.

Here $\psi_s(x)$ are the electron operators at position x for spin $s = \uparrow, \downarrow = +, -$, $p = -i\hbar\partial_x$ is the momentum operator, μ the chemical potential, m the band mass, α_R the Rashba SOI strength, and $\Delta_Z = \mu_B g B_x/2$ the Zeeman interaction strength, with Bohr magneton μ_B and Landé g -factor g . U_{e-e} is a general electron-electron interaction and U_{dis} the disorder potential. $\sigma^{x,z}$ are the spin Pauli matrices, with the spin axes chosen such that α_R couples to σ^z and B_x to σ^x . Equation (1) describes a quantum wire with a single transverse subband, and we exclude the influence of higher subbands.^{14,15} Realizations of Eq. (1) are found in GaAs, InAs,^{11,16,17} Ge/Si,^{18,19} or InSb nanowires.²⁰

Without U_{e-e} and U_{dis} , Eq. (1) leads to the bands shown in Fig. 1. The SOI shifts the \uparrow, \downarrow dispersions by $\pm q_0 = \pm m\alpha_R/\hbar$. The B_x field opens a pseudo-gap at momentum $k = 0$ by spin-flip scattering. We denote the lower (upper) resulting band by a (b). Diagonalizing H leads to the dispersions $E_k^{a,b} = \hbar^2 k^2/2m \mp \sqrt{\Delta_Z^2 + \hbar^2 \alpha_R^2 k^2}$, and the wave functions $|a, k\rangle = u_{-k} |\uparrow\rangle - u_k |\downarrow\rangle$, $|b, k\rangle = u_k |\uparrow\rangle + u_{-k} |\downarrow\rangle$, with $u_k = \left[1 + \hbar\alpha_R k / \sqrt{\Delta_Z^2 + \hbar^2 \alpha_R^2 k^2} \right]^{1/2} / \sqrt{2}$. Overlaps of the form $\langle a/b, k | a/b, k'\rangle$ weight the disorder backscattering amplitudes at a given energy. Figure 2 shows the two overlaps which will be relevant for the localization transition.

III. APPROACH

To study a disordered interacting conductor in 1D, it is generally convenient to bosonize Eq. (1) and use an RG approach. For the present model, however, this approach exhibits some peculiarities. First, the overlap integrals depend on k and the problem is no longer scale invariant, a central assumption for RG. Second, the low-energy physics below the scale set by Δ_Z is described mostly by the band a . Hence, the RG procedure of reducing the en-

ergy scale can lead to a problematic crossing the bottom of the b band, which also invalidates the bosonization formulation that neglects the band curvature. While the exact treatment of every aspect would require a separate investigation, the following two observations allow us to still implement a global RG scheme capturing the relevant physics in a transparent way.

First, Fig. 2 shows that the spin overlaps above Δ_Z approach their asymptotics only slowly with increasing energy E (as $|\langle a, R|a, L \rangle|^2 \sim \Delta_Z^2/2m\alpha_R^2 E$ and $|\langle a, R|b, L \rangle|^2 \sim 1 - \Delta_Z^2/4E^2$). Considering constant overlaps evaluated, e.g., at half of the high energy cutoff scale yields a valid, rather conservative estimate of the true influence of the overlaps. Second, the interactions also renormalize Δ_Z and it grows quickly under the RG flow.^{11,12} Hence the reduced RG bandwidth E meets the growing Δ_Z at a value $E = \Delta_Z^* \gg \Delta_Z$ well above the bottom of the b band, at which the linearity of the bare dispersion remains valid.

Due to these two properties, we propose a unified two-step RG approach to the effect of disorder based on the LL theory. In the first step, we integrate over high energies far above Δ_Z using a constant backscattering overlap and the standard inclusion of the disorder potential.^{3,4} If the disorder is strong enough, localization already occurs in this regime by the conventional backscattering mechanism. Otherwise, at $E = \Delta_Z^*$, we proceed to the second step.

Crossing the gap Δ_Z^* corresponds to freezing out the interaction-generated density fluctuations that renormalize Δ_Z , and hence is not a singular transition through the true band bottom. While the description of the proper transition may be quite challenging, the physics below Δ_Z^* becomes again simple. It is described by a different LL theory for the modes originating from the a band only.^{11,12,21} In this regime it is legitimate to use a larger spin overlap value and, within the accuracy of LL and RG theories, we choose to take the overlaps at the chemical potential μ (see Fig. 2, inset). The evaluation of the disorder backscattering (the second RG step) follows then the standard lines of a spinless LL, and localization occurs if $\xi_{\text{loc}} < \mathcal{L}$.

IV. BOSONIZATION

Above the pseudo-gap, all fluctuations of the a and b bands must be taken into account. As we account for the overlap integrals separately, the standard $s = \uparrow, \downarrow$ basis rather than the a, b basis²² is more convenient for bosonizing. The electron operators are decomposed into R and L moving components as $\psi_s(x) = e^{ik_{FRs}x} \psi_{R,s}(x) + e^{-ik_{FLs}x} \psi_{L,s}(x)$, for k_{FRs}, k_{FLs} the two Fermi points of the (nominal) spin s bands. We then write $\psi_{r,s}(x) = \eta_{r,s} \exp(ri\sqrt{\pi}[\varphi_s(x) + r\vartheta_s(x)]) / \sqrt{2\pi\kappa}$ for $r = R, L = +, -$, the boson fields φ_s and ϑ_s satisfying $[\varphi_{s'}(x'), \partial_x \vartheta_s(x)] = i\delta_{s,s'} \delta(x - x')$, the Klein factors $\eta_{r,s}$, and the short distance cutoff κ . Defin-

ing $\varphi_\rho, \vartheta_\sigma = (\varphi_\uparrow \pm \varphi_\downarrow) / \sqrt{2}$ and $\vartheta_\rho, \varphi_\sigma = (\vartheta_\uparrow \pm \vartheta_\downarrow) / \sqrt{2}$, we obtain the Hamiltonian²² (for $U_{dis} = 0$) $H_{bos} = \sum_{\nu=\rho,\sigma} (u_\nu/2) \int dx [K_\nu^{-1}(\partial_x \varphi_\nu)^2 + K_\nu(\partial_x \vartheta_\nu)^2]$, where $K_{\rho,\sigma}$ measure the interaction strengths ($0 < K_\rho < 1$ for repulsive U_{e-e} and²² $K_\sigma \approx 1$) and $u_{\rho,\sigma}$ are renormalized velocities. Because μ lies in the pseudo-gap, Δ_Z renormalizes as well, expressed by a relevant Hamiltonian $\propto \Delta_Z \cos(\sqrt{2\pi}(\phi_\rho + \theta_\sigma))$, acting on the fields of the b band.^{11,12} We neglect further existing Cooper scattering processes,²² which are overruled by the renormalization of Δ_Z and the disorder here but otherwise would dominate the physics.

The second RG step starts when the growing Δ_Z meets the reduced bandwidth E at $E = \Delta_Z^*$. The b -band fields are then fully gapped,^{11,12} and the low-energy theory is described by the fields related to the a band alone. The corresponding Hamiltonian is obtained from H_{bos} by suppressing all b -related fields, which leads to^{12,21} $H_{bos}^a = (u_a/2) \int dx [K_a^{-1}(\partial_x \varphi_a)^2 + K_a(\partial_x \vartheta_a)^2]$, with $u_a^2 = (1/4) [u_\rho^2 + u_\sigma^2 + u_\rho u_\sigma (K_\rho K_\sigma + K_\rho^{-1} K_\sigma^{-1})]$ and $K_a^2 = K_\rho K_\sigma^{-1} (u_\rho K_\rho + u_\sigma K_\sigma^{-1}) / (u_\rho K_\sigma^{-1} + u_\sigma K_\rho)$. We have neglected here also a marginal coupling between a and b fields¹² because it affects mostly the fermionic response^{21,23} but not the bosonic theory.

V. DISORDER AND RENORMALIZATION GROUP APPROACH

Disorder can be expressed by a random potential U_{dis} with Gaussian distribution^{3,4} that scatters between the bands $i, j = (a/b, L/R)$. The scattering amplitude is described by the dimensionless disorder strength \tilde{D}_{ij} , proportional to the square of the strength of each individual scattering potential, which in turn is proportional to $|\langle i|j \rangle|^2$, hence $\tilde{D}_{ij} = |\langle i|j \rangle|^4 \tilde{D}$. Following the standard replica disorder averaging approach,^{3,4} we obtain the scaling equations (including also the amplitude y expressing bulk backscattering, see Ref. 3)

$$\partial_l K_\rho = -u_\rho K_\rho^2 (2\tilde{D}_{ab} + \tilde{D}_{aa}) / 4u_\sigma, \quad (2)$$

$$\partial_l K_\sigma = -K_\sigma^2 (\tilde{D}_{ab} + y^2) / 2 + \tilde{D}_{aa} / 4, \quad (3)$$

$$\partial_l y = (2 - 2K_\sigma) y - \tilde{D}_{ab}, \quad (4)$$

$$\partial_l \tilde{D}_{aa} = (3 - K_\rho - K_\sigma^{-1}) \tilde{D}_{aa}, \quad (5)$$

$$\partial_l \tilde{D}_{ab} = (3 - K_\rho - K_\sigma - y) \tilde{D}_{ab}, \quad (6)$$

$$\partial_l u_\rho = -K_\rho u_\rho^2 (2\tilde{D}_{ab} + \tilde{D}_{aa}) / 4u_\sigma, \quad (7)$$

$$\partial_l u_\sigma = -u_\sigma K_\sigma \tilde{D}_{ab} / 2 - u_\sigma K_\sigma^{-3} \tilde{D}_{aa} / 4, \quad (8)$$

$$\partial_l \delta(l) = [2 - (K_\rho + K_\sigma^{-1}) / 2] \delta, \quad (9)$$

with l the running RG scale, $\tilde{D}_{aa} = \tilde{D}_{(a,R),(a,L)}$, and $\tilde{D}_{ab} = \tilde{D}_{(a,R),(b,L)}$. We have neglected scattering between $(b, R) \leftrightarrow (b, L)$, $(a, R) \leftrightarrow (b, R)$, $(a, L) \leftrightarrow (b, L)$ after verifying that it has no effect. We have also defined $\delta(l) = \Delta_Z(l)/E(l)$ with $E(l) = \hbar v_F / \kappa(l)$ the running effective bandwidth, for $\kappa(l) = \kappa e^l$ and Fermi velocity

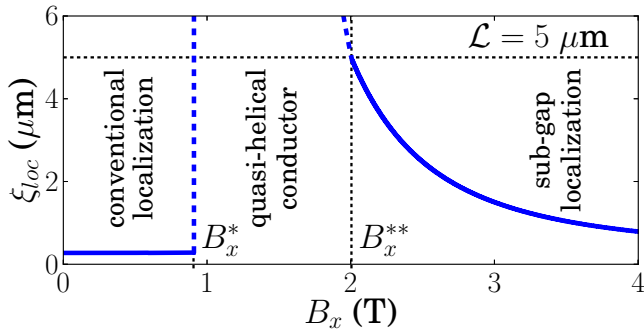


FIG. 3. Localization length ξ_{loc} of an InAs nanowire as a function of B_x for $\tilde{D} = 0.01$ and $\mathcal{L} = 5 \mu\text{m}$. Close to $B_x = 0$ the system is localized due to conventional backscattering. At $B_x \sim B_x^* \approx 0.9$ T the system crosses over to a quasi-helical conductor and at $B_x \sim B_x^{**} \approx 2$ T to a localized phase due to sub-gap backscattering. The transition at B_x^* results from the competition of the renormalization of Δ_Z and \tilde{D}_{ab} and is thus expected to be quite abrupt and independent of \mathcal{L} . The transition at B_x^{**} is a strongly \mathcal{L} dependent cross-over.

v_F .¹² The latter equations express the competition between disorder backscattering and the delocalizing effect by repulsive interactions³ and by B_x induced spin-flip scattering. Localization occurs when the latter is not strong enough such that $\tilde{D}_{ab} \sim 1$ (\tilde{D}_{aa} remains small above the gap) before we reach $E = \Delta_Z^*$ ($\delta(l) \sim 1$) or $\kappa(l) > \mathcal{L}$. Otherwise we switch to the second step, described by H_{bos}^a , with the parameters K_a and u_a obtained from the resulting $K_{\rho,\sigma}, u_{\rho,\sigma}$ of the first step. As argued above, the spin overlap weighting \tilde{D}_{aa} can now (discontinuously) be replaced by $\langle a, L | a, R \rangle$ evaluated at $E = \mu$. The RG equations are

$$\partial_l K_a = -K_a^2 \tilde{D}_{aa} / 2, \quad (10)$$

$$\partial_l \tilde{D}_{aa} = (3 - 2K_a) \tilde{D}_{aa}, \quad (11)$$

$$\partial_l u_a = -u_a K_a \tilde{D}_{aa} / 2, \quad (12)$$

describing, for effectively spinless fermions, the competition between localization and delocalizing superconducting fluctuations.³ The latter overrule disorder localization above the critical attractive interaction strength³ $K_a > 3/2$. However, $K_a < 1$ for repulsive interactions, disorder scattering is relevant, and localization occurs if $\tilde{D}_{aa} \sim 1$ is reached while $\kappa(l) < \mathcal{L}$; otherwise the (finite) system is a helical conductor.

VI. RESULTS AND DISCUSSION

To give a definite example, we focus on InAs nanowires,^{11,24} using $\alpha_R = 4 \times 10^{-11}$ eV m, $g = -9$, $m = 0.040m_e$ (with electron mass m_e), $v_F = 2 \times 10^5$ m/s, $u_\rho = v_F/K_\rho$ and $u_\sigma = v_F/K_\sigma$, with $K_\rho = 0.5$, $K_\sigma = 1$, $y = 0.1 |\langle aL | bR \rangle|^2$, and short length cutoff $\kappa = 15$ nm (which is longer than the lattice constant $a_0 = 6.06 \text{ \AA}$,

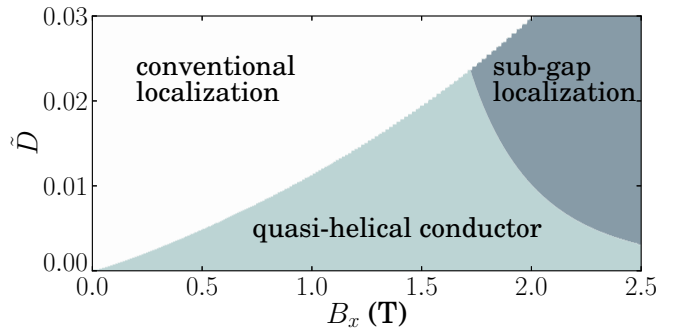


FIG. 4. Phase diagram for InAs nanowires obtained from curves as in Fig. 3 for various \tilde{D} . At $\tilde{D} > 0.023$ the quasi-helical phase is suppressed and there is a direct crossover between the localized phases. Not visible on the shown scale is the localization threshold for $B_x = 0$, occurring at $\tilde{D} \approx 0.003$.

and expresses a smaller effective bandwidth). The localization length is $\xi_{\text{loc}} = \min_{ij} \kappa(l^*) / \tilde{D}_{ij}(l^*)$ with $l = l^*$ the scale at which the RG flow stops (in the first or the second step). If a $\tilde{D}_{ij}(l^*) = 1$ is reached before $\kappa(l) > \mathcal{L}$, the system is localized, $\xi_{\text{loc}} < \mathcal{L}$. We consider disorder strengths about $\tilde{D} \sim 0.01$, leading at $B_x = 0$ to $\xi_{\text{loc}} \sim 0.3 \mu\text{m}$. For a sample length of, e.g., $\mathcal{L} = 5 \mu\text{m}$, the system is well localized. At small fields, the \tilde{D}_{ab} and B_x scattering processes compete, and if B_x passes a critical value $B_x < 1$ T, $\Delta_Z(l)$ overrules the disorder backscattering and the system becomes a quasi-helical conductor, where $\xi_{\text{loc}} > \mathcal{L}$ is now determined by the sub-gap disorder strength \tilde{D}_{aa} . At $B_x = B_x^{**} \sim 2$ T, $|\langle a, R | a, L \rangle|$ becomes large enough such that $\xi_{\text{loc}} < \mathcal{L}$ and the system crosses over into the sub-gap localized phase. In Fig. 3 we plot this crossover behavior for $\tilde{D} = 0.01$. Tracing similar curves for various disorder strengths \tilde{D} leads to the phase diagram shown in Fig. 4. For strong disorder, the quasi-helical conduction phase is absent, and the crossover takes place directly between the two localized phases.

To conclude, we note that the disordered quasi-helical system shows at B_x^* a phase transition from the conventional Anderson localized phase in which ξ_{loc} only weakly increases with B_x , to a phase in which ξ_{loc} jumps to a very large value and then decreases with increasing B_x . For fields $B_x^* < B_x < B_x^{**}$, ξ_{loc} exceeds \mathcal{L} and forms a quasi-helical conductor before crossing over into another localized phase. While the former localized phase is characterized by the conventional $2k_F = 2q_0$ modulated charge density wave, the latter sub-gap localized phase combines a $4q_0$ density wave with a uniform electron polarization as the order parameter. The existence of a quasi-helical conduction state between the two insulating phases as a function of B_x is a peculiar behavior that could be used to test if a conductor is helical. Remarkably the conducting phase extends into the regime of quite strong disorder, which indicates that a quasi-helical conductor does not necessarily require ultraclean

samples. The boundaries of this phase in the phase diagram are controlled predominantly by Δ_Z , and so the g -factor of the material has the largest influence on the phase diagram. For instance, a similar phase diagram as Fig. 4 for InSb with²⁰ $g \approx 50$ spans over $B_x = 0 - 0.1$ T and $\bar{D} = 0 - 0.002$.

ACKNOWLEDGMENTS

We thank F. Assaad, D. Baeriswyl, H. Johannesson, and P. Recher for valuable discussions. B.B. acknowledges the support by the EU-FP7 project SE2ND [271554]. A.S. acknowledges the support by the Swedish research council, Grant No. 621-2011-3942. G.I.J. acknowledges the support by the Georgian NSF Grant No. ST09/4-447 and by the SCOPES Grant IZ73Z0-128058.

-
- ¹ P. W. Anderson, Phys. Rev. **109**, 1492 (1958).
² N. F. Mott, Rev. Mod. Phys. **40**, 677 (1968); P. A. Lee and T. V. Ramakrishnan, Rev. Mod. Phys. **57**, 287 (1985); B. Kramer and A. MacKinnon, Rep. Prog. Phys. **56**, 1469 (1993); D. Belitz and T. R. Kirkpatrick, Rev. Mod. Phys. **66**, 261 (1994); G. Modugno, Rep. Prog. Phys. **73**, 102401 (2010); E. Abrahams (ed.), *50 Years of Anderson Localization* (World Scientific, Singapore, 2010).
³ T. Giamarchi, *Quantum Physics in One Dimension*, (Oxford University Press, Oxford, 2003).
⁴ T. Giamarchi and H. J. Schulz, Phys. Rev. B **37**, 325 (1988).
⁵ C. Wu, B. A. Bernevig, and S. C. Zhang, Phys. Rev. Lett. **96**, 106401 (2006); A. Ström, H. Johannesson, and G. I. Japaridze, Phys. Rev. Lett. **104**, 256804 (2010).
⁶ M. König, H. Buhmann, L. W. Molenkamp, T. Hughes, C.-X. Liu, X.-L. Qi, and S.-C. Zhang, J. Phys. Soc. Japan, **77**, 031007 (2008); M. Z. Hasan and C. L. Kane, Rev. Mod. Phys. **82**, 3045 (2010).
⁷ P. Štréda and P. Šeba, Phys. Rev. Lett. **90**, 256601 (2003).
⁸ J. Klinovaja, M. J. Schmidt, B. Braunecker, and D. Loss, Phys. Rev. Lett. **106**, 156809 (2011); Phys. Rev. B **84**, 085452 (2011).
⁹ K. Sato, D. Loss, and Y. Tserkovnyak, Phys. Rev. Lett. **105**, 226401 (2010); Phys. Rev. B **85**, 235433 (2012).
¹⁰ For a review of the recent developments see: J. Alicea, Rep. Prog. Phys. **75**, 076501 (2012).
¹¹ B. Braunecker, G. I. Japaridze, J. Klinovaja, and D. Loss, Phys. Rev. B **82**, 045127 (2010).
¹² B. Braunecker, P. Simon, and D. Loss, Phys. Rev. Lett. **102**, 116403 (2009); Phys. Rev. B **80**, 165119 (2009).
¹³ A. Soori, S. Das, and S. Rao, Phys. Rev. B **86**, 125312 (2012).
¹⁴ M. Governale and U. Zülicke, Phys. Rev. B **66**, 073311 (2002); Solid State Commun. **131**, 581 (2004).
¹⁵ A. Schulz, A. De Martino, P. Ingenhoven, and R. Egger, Phys. Rev. B **79**, 205432 (2009).
¹⁶ S. Nadj-Perge, S. M. Frolov, J. W. W. van Tilburg, J. Danon, Y. V. Nazarov, R. Algra, E. P. A. M. Bakkers, and L. P. Kouwenhoven Phys. Rev. B **81** 201305(R) (2010).
¹⁷ H. Shtrikman, R. Popovitz-Biro, A. V. Kretinin, and P. Kacman, IEEE J. Sel. Top. Quantum Electron. **17**, 922 (2011).
¹⁸ C. Kloeffel, M. Trif, and D. Loss, Phys. Rev. B **84**, 195314 (2011).
¹⁹ X.-J. Hao, T. Tu, G. Cao, C. Zhou, H.-O. Li, G.-C. Guo, W. Y. Fung, Z. Ji, G.-P. Guo, and W. Lu, Nano Lett. **10**, 2956 (2010).
²⁰ S. Nadj-Perge, V. S. Pribiag, J. W. G. van den Berg, K. Zuo, S. R. Plissard, E. P. A. M. Bakkers, S. M. Frolov, and L. P. Kouwenhoven, Phys. Rev. Lett. **108**, 166801 (2012).
²¹ B. Braunecker, C. Bena, and P. Simon, Phys. Rev. B **85**, 035136 (2012).
²² S. Gangadharaiah, J. Sun, and O. A. Starykh, Phys. Rev. B **78**, 054436 (2008).
²³ D. Schuricht, Phys. Rev. B **85**, 121101 (2012).
²⁴ C. Fasth, A. Fuhrer, L. Samuelson, V. N. Golovach, and D. Loss, Phys. Rev. Lett **98**, 266801 (2007).